Constraining the timing of palaeosol development in Iranian arid environments using OSL dating

Rashidi, Zakieh; Sohbati, Reza; Karimi, Alireza; Farpoor, Mohammad Hadi; Khormali, Farhad; Thompson, Warren; Murray, Andrew Sean

Published in:
Quaternary Geochronology

Link to article, DOI:
10.1016/j.quageo.2018.04.006

Publication date:
2019

Document Version
Peer reviewed version

Accepted Manuscript

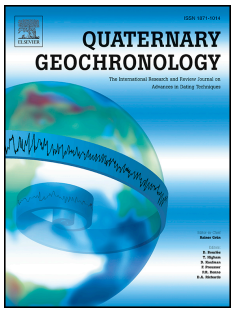

Constraining the timing of palaeosol development in Iranian arid environments using OSL dating

Zakieh Rashidi, Reza Sohbati, Alireza Karimi, Mohammad Hadi Farpoor, Farhad Khormali, Warren Thompson, Andrew Murray

PII: S1871-1014(17)30237-6

DOI: 10.1016/j.quageo.2018.04.006

Reference: QUAGEO 917

To appear in: *Quaternary Geochronology*

Received Date: 7 December 2017

Revised Date: 11 March 2018

Accepted Date: 11 April 2018

Please cite this article as: Rashidi, Z., Sohbati, R., Karimi, A., Farpoor, M.H., Khormali, F., Thompson, W., Murray, A., Constraining the timing of palaeosol development in Iranian arid environments using OSL dating, *Quaternary Geochronology* (2018), doi: 10.1016/j.quageo.2018.04.006.

Constraining the timing of palaeosol development in Iranian arid environments using OSL dating

Zakieh Rashidi[1-2], Reza Sohbati[3], Alireza Karimi[1*], Mohammad Hadi Farpoor[4], Farhad Khormali [5], Warren Thompson[2], Andrew Murray[2]

[1]Department of Soil Science, Faculty of Agriculture, Ferdowsi University of Mashhad, Mashhad, 91779-48978, Iran

[2]Nordic Laboratory for Luminescence Dating, Department of Geoscience, Aarhus University, DTU Risø Campus, DK-4000, Roskilde, Denmark

[3]Technical University of Denmark, Centre for Nuclear Technologies, DTU-Nutech, DTU Risø Campus, DK-4000, Roskilde, Denmark

[4]Department of Geological Sciences, Bahonar University of Kerman, Iran

[5] Department of Soil Sciences, Gorgan University of Agricultural Sciences and Natural Resources, Iran

*Corresponding author: karimi-a@um.ac.ir

Constraining the timing of palaeosol development in Iranian arid environments using OSL dating

Abstract

The ages of palaeosols in arid environments in Iran are constrained using the optically stimulated luminescence (OSL) signal from quartz. The luminescence properties of quartz OSL and K-feldspar infrared stimulated luminescence (IRSL) at 50°C (IR_{50}) and post-IR IRSL at 290°C ($pIRIR_{290}$) signals are compared to investigate the degree of bleaching of quartz OSL in individual samples at the time of deposition. A comparison between the quartz OSL and K-feldspar IR_{50} ages shows that 12 out of 15 samples were probably well-bleached prior to deposition. The 17 OSL ages constrain at least four broad phases of sediment deposition and soil formation on the central Iranian plateau: (i) prior to, and (ii) during, mid/late MIS 5 (at Isfahan and Lar), (iii) MIS 3 (at Bam, Mahan and probably Isfahan) and (iv) MIS 1 (at Rayen and Jiroft). In summary, there is no convincing evidence for palaeosol formation during MIS 4 and MIS 2; however pedogenesis does appear to have taken place during all other marine isotope stages over the last full glacial-interglacial cycle.

Keywords: Chronostratigraphy; Luminescence dating; Palaeoclimate; Bleaching; Marine isotope stage; Quartz OSL

1. Introduction

Establishing a chronological framework is of crucial importance to palaeoclimate and landscape evolution studies. Without any knowledge of the timing of environmental change, understanding environmental history is not possible. Palaeosols are important archives for reconstruction of past climates and environments (e.g. Retallack, 2001); they are formed in response to environmental changes and can be used as records for understanding palaeoclamatic conditions. Palaeosols in various sediment sequences such as alluvial (e.g. Kemp et al., 2006), aeolian (e.g. Wang et al., 2016), marginal marine strata and even glacial deposits (e.g. Mahaney et al., 2013) are reliable indicators for stablishing a chronostratigraphic subdivision and correlation with marine isotope stages (MIS) and glacial-interglacial cycles (e.g. Gornitz, 2008). Palaeosols developed in alluvial deposits have the potential of providing information on episodes of landscape instability (sediment deposition), stability (soil development) and landscape evolution (Kraus, 1999).

The palaeoclimate records of Iran have been subject to several studies over the last decade (e.g. Karimi et al., 2009; Kehl, 2010; Khormali and Kehl, 2011). Quaternary events in Iranian plateau present important records of palaeoenvironmental changes in the arid environments of the Middle East. They can be seen as a valuable link for correlating Europe and Central Asia through the deserts of Saudi Arabia to the West and the deserts of Central Asia to the East; providing an understanding of palaeoenvironment and landscape evolution resulting in the genesis of the Old World Dry Belt (Kehl, 2010).

Most of the palaeoclimatic studies in Iran have been based on geomorphic and pedogenic evidence (e.g. Karimi et al., 2009; Khormali and Kehl., 2011; Farpoor et al., 2012; Ghafarpour et al., 2016). A few studies have applied absolute dating methods to studying palaeoenvironmental and landscape change in Iran (Kehl et al., 2005; Frechen et al., 2009; Karimi et al., 2011; Lauer et al., 2016; Büdel et al., 2017), but most focus on the loess-

palaeosol sequences of Northern and Northeast of Iran (e.g. Frechen et al., 2009; Karimi et al., 2011; Lauer et al., 2016). Some of these studies suggest that well-developed palaeosols correlate with the last interglacial (MIS 5) or MIS 7 and older interglacials (Frechen et al., 2009; Lauer et al., 2016). Additionally, they suggest loess accumulation during last glacial period MIS 2 (Karimi et al., 2011).

In a recent study in northern Iran, stratigraphic results of Agh Band loess-palaeosol show poorly- as well as well-developed palaeosol horizons formed around 80 ka and late MIS 7-MIS 6 with increased humidity and landscape stability (Lauer et al., 2016). In southern Iran, apart from two studies (i.e. Kehl et al., 2005; Kehl et al., 2009), no information is available on the various phases of soil formation and sediment deposition. According to Kehl et al. (2005), based on the stratigraphy and different degrees of soil development, the well-developed Bw(t) and Btk horizons in the Persepolis basin, reflect probable soil-forming periods during MIS 5, while the upper loess deposits were likely formed under considerably cooler and drier climatic conditions during the LGM. The poorly-developed horizons indicate interstadial periods of MIS 3 and short phases of climate amelioration during the early Holocene.

It appears that there is little information available from the dry zones of Iranian plateau to allow the reconstruction of palaeoenvironment based on the timing of sediment deposition-soil formation sequences. This is partly due to the lack of reliable chronological control in the studies in this area. Alluvial fans and pediments are the most common landforms in the arid regions of Iran. The most developed soil horizon identified in these landforms is a Btk horizon in both buried and relict forms. Morphological, micromorphological and mineralogical characteristics of the palaeosols developed in these landforms have been previously described (Khademi and Mermurt, 1999; Khormali et al., 2003; Sanjari et al., 2011; Nejad Zamani., 2014). These studies investigated the pedogenesis of these arid-region

74 soils using various techniques. Unfortunately, none of these studies provides quantitative
75 information on the timing of palaeosol development. Indeed, in the Middle East in general,
76 the timing of sedimentation and pedogenesis in alluvial sediment is not well documented.
77 Given the similarity of palaeosols in the arid areas in Iran, an overall understanding of the
78 timing of sedimentation and soil genesis episodes is very desirable. Here, we attempt to
79 establish a first instrumental chronology for pedosedimentary events associated with
80 previously identified palaeosols; these developed in alluvial fans and pediments in the arid
81 areas of the Iranian plateau. Luminescence dating is used to set the first chronological
82 constraints on the palaeosols, by determining the time at which the sediments, in which the
83 palaeosols later formed, were deposited. Optically stimulated luminescence (OSL) is a well-
84 established absolute dating method that determines the time elapsed since sediment grains
85 were last exposed to daylight. In this method, quartz and feldspar grains act as natural
86 dosimeters and can potentially yield ages of sediment deposition ranging from a few years to
87 few hundred thousands of years. Many studies have made use of luminescence dating to
88 establish a chronology for sedimentation and soil formation processes (e.g. Murray and
89 Clemmensen, 2001; Leopold et al., 2011; Hal and Goble, 2015). In an attempt to establish a
90 chronology for soil development, we apply luminescence dating to six different soil profiles
91 in arid alluvial settings in Central Iranian plateau.

92 **2. Study area and sampling**

93 The Iranian Plateau is located in southwest Asia, between the Persian Gulf and the Oman Sea
94 to the south and the Caspian Sea to the north (Darehshouri and Kasraian, 1998) (Fig. 1a). The
95 study sites are located at six different geographical areas in the centre, east and southeast of
96 the Iranian plateau (Fig. 1a). The present-day average annual precipitation and temperature
97 range from 145 to 200 mm and from 14°C to 24.5 °C, respectively, thus the overall climate of
98 the study area is considered arid.

All our sections are located in alluvial and fluvial landforms and are physiographically similar (Table 1). Each section includes a representative pedon identified and logged in alluvial or fluvial deposits that originated from adjacent highlands. The location and environmental characteristics of sections are described in Table 1. These pedons consist of a sequence of palaeosol-sediment or a sequence of poorly- and well-developed palaeosols (Fig. 1b). The studied pedons and their sediment origins have long geological history, spanning from Miocene to present and Cretaceous to Pliocene, respectively. Because the most part of the Iranian plateau is covered by limestone formations, the parent material of most of the pedons studied here are calcareous; dominated by limestone and marl. The representative pedons were described and soil horizons identified according to the criteria of the Soil Survey Staff (2014).

In total, seventeen samples were collected for luminescence dating by hammering metal tubes (5 cm diameter and 15 cm long) into freshly exposed section walls: (i) twelve samples from well-developed palaeosols, (ii) two samples from less developed palaeosols, and (iii) three samples from sediment layers without or with very little pedogenic material (Fig. 1b). At each site (except for Isfahan where the ground surface was reworked by agricultural activity), an additional sample was collected by brushing the very top surface (< 2 cm) of the ground into aluminium foil which was then wrapped and sealed in light-tight bags. Such modern analogues were taken to estimate the degree of bleaching (i.e. residual dose) in currently-exposed samples. In addition to the luminescence samples, ~250 grams of material from around each tube was collected for annual dose rate measurements.

3. Sample preparation and analytical facilities

Sediment was removed from sampling tubes under subdued orange light. Material from the exposed ends was saved for water content measurements and sediment from the middle (unexposed) part of the tubes was wet sieved to 125–250 µm. This fraction was then treated

with 10% HCl to remove carbonates. The presence of gypsum in some of the samples presented a challenge in sample preparation; gypsum dissolves in water very slowly. To accelerate this dissolution, we treated the samples with a mixture of citric acid and propanol repeatedly until all or the majority of gypsum was removed. The samples were subsequently treated by 10% H_2O_2 to remove any reactive organic material, followed by 10% HF for 40 min. to remove any alpha-irradiated surface layer and weathering products and coatings, and 10% HCl for 20 min. to remove any fluoride precipitation. The K-rich feldspar fractions were separated by suspension in a water-based heavy liquid solution (ρ=2.58 g.cm^{-3}; Fastfloat). The denser (settled) quartz grains (ρ > 2.58 g.cm^{-3}) were further treated with concentrated (40%) HF for 60 min. followed by 10% HCl for 40 min..

All luminescence measurements were carried out using a Risø TL/OSL reader (model TL-DA 20), with blue light stimulation (470 nm, ~80 mW.cm^{-2}) and photon detection through a 7.5-mm Hoya U-340 glass filter for quartz, and infrared stimulation (875 nm, ~135 mW.cm^{-2}) and photon detection through a Schott BG39/BG3 filter combination (2 and 3mm, respectively) for K-feldspar (Bøtter- Jensen et al., 2010). Beta irradiations used a ^{90}Sr/^{90}Y source mounted on the reader and calibrated for both discs and cups using 180–250 µm calibration quartz grains (Hansen et al., 2015). Grains were mounted as large (9 mm diameter for quartz) or medium (~4 mm diameter for feldspar) aliquots in a monolayer on 9-mm-diameter stainless steel discs (quartz) or cups (feldspar) using silicone oil. The heating rate was 5 °C.s^{-1} throughout. All thermal treatments and stimulations at temperatures higher than 200 °C were carried out in nitrogen atmosphere, and a pause of 5 s was inserted before stimulation to allow all grains to reach the measurement temperature. Five empty channels were inserted before and after the stimulation to monitor any isothermal TL signals.

4. Dosimetry

Radionuclide concentrations (^{238}U, ^{232}Th and ^{40}K) were measured using high-resolution gamma spectrometry. The additional sediment sample collected from around each metal tube was first dried at 50 ^{o}C. A subsample of ~250 g was pulverized and homogenized, and then heated to 450 ^{o}C for 24 h to remove any organic matter. The material was then cast in wax to prevent radon loss and to provide a reproducible counting geometry. Samples were stored for at least three weeks to allow ^{222}Rn to reach equilibrium with its parent ^{226}Ra before being measured on a high-purity Germanium detector for at least 24 h. Details of the gamma spectrometry calibration are given in Murray et al. (1987). The internal beta dose rate from ^{40}K to feldspar grains was calculated based on an assumed effective potassium content of 12.5±0.5% (Huntley and Baril, 1997), and the beta contribution from ^{87}Rb was calculated assuming a ^{87}Rb content of 400±100 ppm (Huntley and Hancock, 2001). A small internal alpha contribution of 0.10±0.05 Gy ka^{-1} from internal ^{238}U and ^{232}Th was also included in the dose rates, derived from ^{238}U and ^{232}Th concentration measurements by Mejdahl (1987). For quartz, an internal dose rate of 0.010±0.002 Gy.ka^{-1} was assumed (Vandenberghe et al., 2008). The radionuclide concentrations were converted to dose rate data using the conversion factors from Guerin et al. (2011). The cosmic-ray dose rates were calculated according to Prescott and Hutton (1994), assuming an uncertainty of 5%. The long-term water content of each sample was estimated based on the field water content and saturation water content as well as the probable position of the water table during the burial time. All radionuclide concentrations, water contents and dose rates are summarized in Table 2.

5. Luminescence characteristics and dose measurements

5.1. Quartz

All the OSL measurements were performed at 125 ^{o}C for 40s using a single-aliquot regenerative (SAR) protocol (Table S1; Murray and Wintle, 2000). A high-temperature blue light stimulation at 280 ^{o}C was applied at the end of each cycle to reduce recuperation (Table

S1; Murray and Wintle, 2003). Values for L_x and T_x were derived from the initial 0.16 s of the signal minus an immediate background derived from the following 0.16 s. An early background subtraction was used to minimize the possible effect of the more difficult to bleach and more thermally unstable medium and slow components (Jain et al., 2003; Li and Li, 2006; Cunningham and Wallinga, 2010).

For all the samples, the purity of quartz extracts was examined by measuring the OSL signal from three aliquots from each sample with and without prior IR stimulation at room temperature for 100 s. The ratio of the two signals, the so-called OSL-IR depletion ratio, was then calculated for each aliquot (Duller, 2003). The resulting average OSL-IR depletion ratio was 0.90±0.03 (n = 51), implying that any feldspar contamination in our quartz OSL signal is not significant. Quartz extracts from all the samples were sensitive and the OSL signal was dominated by the fast component (Fig. 2a, inset). Figure 2a shows a typical dose-response curve for sample 177118, fitted with a saturating exponential function; the sensitivity-corrected signals are reproducible (recycling ratio is close to unity), the dose-response curve passes through the origin (recuperation is small) and the D_e for this aliquot is ~111 Gy.

Both natural and dose recovery preheat plateau tests were performed to determine the appropriate measurement conditions. The natural preheat-plateau test was carried out to investigate the dependence of equivalent dose (D_e) on preheat temperature. Twenty-one aliquots of quartz from sample 177118 were sorted into groups of three. The D_e was measured with different preheat temperatures for each group, in steps of 20°C ranging from 180°C to 300°C (held for 10 s). The temperature of the cut heat was chosen to be 40 °C lower than that of the first preheat treatment. From Fig. 2b it can be seen that there is no systematic dependence of D_e on preheat temperature between 180 and 300 °C.

Similarly, the dose-recovery preheat-plateau test was carried out on 21 fresh aliquots of sample 177118. The natural OSL signal was removed by two blue stimulations for 100 s at

198 room temperature. A pause of 10000 s was used between the two stimulations to allow any
199 charge trapped in shallow refuge traps (especially that associated with the 110 °C TL peak) to
200 decay and subsequently partly refill the OSL trap before the second stimulation. The aliquots
201 were then given a laboratory dose of ~75 Gy and measured in a similar manner as in the
202 natural preheat plateau test. Figure 2c illustrates the results of measured to given dose ratios
203 at different preheat temperatures. As with the D_e preheat plateau, no systematic dependence
204 of dose recovery ratio on preheat temperature is observed. The average dose recovery ratio is
205 1.06±0.04 (n=21), showing that a known laboratory dose given to the sample before any
206 thermal treatment can be measured accurately. Based on these results, we selected a preheat
207 temperature of 240 ^{o}C, and undertook a further dose recovery tests on all the samples at this
208 temperature; the overall dose recovery ratio is 0.88±0.05 (n = 51; inset to Fig. 2c). There is a
209 large scatter in these data; the dose recovery ratios vary from 0.26 to 2.7 (inset to Fig. 2c).
210 Nevertheless, for all quartz OSL measurements described below a preheat/cutheat
211 temperature of 240/200°C was used, although we further investigate the possible effect of
212 this very variable dose recovery ratio on our quartz OSL ages in Section 6.

213 **5.2. K-rich feldspar**

214 A $pIRIR_{290}$ protocol was adopted to measure the K-feldspar fractions (Buylaert et al., 2012).
215 The D_e was measured using a SAR protocol with a preheat of 320 °C for 60 s after both
216 regenerative and test doses. The first IR stimulation at 50 °C was followed by a second IR
217 stimulation at 290 °C. A high-temperature stimulation at 325 °C was also given at the end of
218 each SAR cycle to minimise any build-up of charge giving rise to a recuperated signal. All IR
219 stimulations were carried out for 100 s (Table S1). The pIRIR signals were derived from the
220 first 1 s of the IR stimulation with a subtracted background based on the last 10 s. Test dose
221 values were chosen to be ~25% of the $pIRIR_{290}$ D_e estimates for all samples. All dose
222 response curves were fitted with a single saturating exponential function.

6. Quartz OSL ages and bleaching

The quartz OSL ages of all the pedons are summarised in Fig.1b. The ages range from 5.2±0.6 ka for the sediment in which a poorly-developed palaeosol (Bk) has formed at the Jiroft section to 107±11 ka for the sediment containing a well-developed Btky2 palaeosol at Isfahan section. The sediment ages at all sections are in stratigraphic order except at Isfahan where the age of the bottom Btky3 layer is younger than both the age of the immediately overlying Btky2 layer, and the unit above, containing Btky1. We do not consider the age of the bottom unit in the discussion below because it is younger than both the overlying samples and because the equivalent dose of the immediately overlying sample 177120 is ~150 Gy (i.e. approaching saturation). It is well-known that quartz close to saturation tends to underestimate age (Chapot et al., 2012) and so it is not surprising that the age of the bottom sample is underestimated.

In the luminescence dating of samples from alluvial settings, one must always consider the possibility of incomplete resetting or bleaching of the signal before final deposition. The bleaching rate may be a function of several parameters such as water depth, sediment load, turbulence, light spectrum, grain size, and transport distance (e.g. Jain et al., 2004). To investigate the likely importance of incomplete bleaching, we use two approaches: i) we determine the residual dose in modern analogues, and ii) look at the relative doses recorded by two signals that bleach at different rates.

6.1. Modern analogue

One way to evaluate the significance of incomplete bleaching is to estimate the residual doses in currently-exposed deposits at the sampling site (e.g. Murray and Olley, 2002; Jain et al., 2004; Porat et al., 2010). Such modern analogues can provide useful information on the likely degree of bleaching in the fossil samples prior to deposition. Eighteen aliquots of quartz and twelve aliquots of K-feldspar were measured on material extracted from samples of

identifiably modern sediment from 5 sites. Table 3 summarizes the quartz OSL and K-feldspar IR_{50} and $pIRIR_{290}$ D_e values of modern analogues from these sites. No representative modern analogue was available at Isfahan section due to significant soil surface disturbance by agricultural activity. The quartz OSL residual doses range from ~0.1 Gy (at Bam, Lar and Mahan) to ~1.6 Gy (at Rayen). The largest IR_{50} and $pIRIR_{290}$ doses are ~2 Gy (at Mahan) and ~5 Gy (at Rayen), respectively. All these doses are small compared to the equivalent doses measured in the fossil samples from the corresponding site, suggesting that the fossil samples were likely to have been sufficiently bleached at the time of deposition.

6.2. K-feldspar versus quartz

Several studies have shown that the quartz OSL signal resets more rapidly than feldspar IR_{50} signal (e.g. Godfrey-Smith et al., 1988) and that the IR_{50} signal, in turn, bleaches more quickly than the $pIRIR_{290}$ signal (e.g. Murray et al., 2012). Unfortunately sufficient feldspar was not available from some samples, but Fig. 3a summarises the dose measurement made on the 15 samples for which sufficient material could be extracted (all sites). This plot of the IR_{50} versus $pIRIR_{290}$ equivalent doses shows that most data points are consistent with a straight line (Fig. 3a) of slope 0.47±0.02. Given the heterogeneous nature of the bleaching process in space and time, the relatively constant relationship over a wide dose range implies that the feldspar signals in most of our samples are likely to have been well-bleached prior to deposition (e.g. Sohbati et al., 2016).

Based on the differential bleaching of quartz OSL and K-feldspar IRSL signals, Murray et al. (2012) proposed an approach to identifying well-bleached quartz by comparing quartz OSL with feldspar IR_{50} and $pIRIR_{290}$ ages. Following a similar approach, a comparison between the quartz OSL and the K-feldspar IR_{50} ages shows that, except for three samples (at Jiroft profile), the IR_{50} ages are comparable to or younger than the corresponding quartz ages (Fig. 3b, Table 2), with an average IR_{50} to quartz age ratio of 0.58±0.04, consistent with the degree

of fading expected for the IR_{50} signal, and suggesting that the quartz OSL signal in these samples is likely to have been well-bleached prior to deposition (all these samples are identified as 'probably well-bleached' in Table 2). The IR_{50} signal from the three samples from the Jiroft profile has apparently not been as well-bleached as those from the other profiles, and thus we do not know if the quartz signal in these samples was sufficiently reset. We also compared the quartz OSL ages with the $pIRIR_{290}$ ages. Figure 3c shows that the $pIRIR_{290}$ ages for 6 of the samples are consistent with the corresponding quartz OSL ages (identified as 'well-bleached' in Table 2); the remaining (including the 3 from the Jiroft profile) overestimate. This implies that despite the negligible $pIRIR_{290}$ residual doses in the modern analogues and the correlation between the IR_{50} and $pIRIR_{290}$ over a wide dose range (Fig. 3a), the $pIRIR_{290}$ signal in some of our samples may not have been sufficiently bleached prior to deposition.

6.3. Does quartz dose recovery affect the OSL ages

In order to see whether the apparent difficulty in recovering a known dose for some aliquots (inset to Fig. 2c) is systematically affecting the measurement of dose in quartz, we compare the OSL to IR_{50} age ratio with the quartz OSL dose recovery ratio for all the samples. Figure 3d shows that there is no correlation between the two ratios. Thus, the unsatisfactory dose recovery ratios observed for some of the samples does not seem to lead to a detectable systematic underestimation of the quartz age, as might otherwise have been expected. Since our quartz OSL ages do not seem to be affected either by poor dose recovery or by incomplete bleaching (with the possible exception of the Jiroft profile) the quartz ages are used in the geological interpretation of the next section.

7. Discussion

The Jirof section provides three OSL ages of between 5.2±0.6 and 15±2 ka. These OSL age estimates indicate the time of sediment deposition and so suggest that soil development

started after 15 ka ago, and was ongoing until at least the middle of the Holocene (although the youngest unit has only a poorly-developed soil). However, none of these 3 samples are identified as well- or probably-well bleached by comparison between the quartz OSL age and the feldspar ages, and so the calculated ages may be overestimates (marked with a (?) in Table 2).

The two samples from Rayen section give OSL age estimates of 5.5±0.5 ka for a sediment with no significant soil development 60 cm below the surface, and 26±3 ka for the most developed Btk horizon at 115 cm; the 2 OSL ages are identified in Table 2 as well bleached and probably well bleached, respectively. It appears that alluvial deposition of this pedon took place before or around the LGM, and that soil formation took place later, resulting in a well-developed Btk horizon in depth of 115 cm. Further alluvial sediments were deposited at 5.5±0.5 ka (MIS 1), and no significant soil development took place in this unit, constraining the period of soil development in the underlying unit to between 26±3 and 5.5±0.5 ka. The sharp transition between the lower well-developed soil horizon and the upper underdeveloped deposits suggests a chronological discontinuity in this pedon, for instance arising from an erosion event.

Finally, the uppermost unit at Mahan contains a well-developed Bt palaeosol in a sediment with a deposition age of 18.5±1.5 ka, and identified in Table 2 as well bleached. Although less well-constrained than at Jiroft and Rayen, this palaeosol may also have developed during the Holocene.

These results suggest that 5 units (3 at Jiroft, 1 at Rayen and 1 at Mahan) probably all developed soils to various degrees during the Holocene. The presence of a 5.5±0.5 ka sediment cap at Rayen and only a weakly-developed soil in the youngest unit at Jiroft probably constrains the active soil development period to the early/mid Holocene.

The stratigraphy and soil horizons recorded in the Bam pedon appear similar to those in the Rayen pedon, but deposition occurred much earlier, at 61±5 ka (MIS 4), indicating soil formation probably after MIS 4. The age of the sample taken from upper coarse-grained deposits is 9.1±0.9 ka, substantially younger than the underlying sediment; this constrains the formation of this soil most likely to MIS 3, although soil formation in MIS 2 cannot be ruled out purely on stratigraphic grounds. The time gap between the two horizons may indicate an erosional event, possibly during MIS 2. One of the two samples appears to have been well reset, and the other probably well reset (Table 2).

The palaeosol-sediment sequence at Mahan gives stratigraphically consistent OSL age estimates ranging from 18.5±1.5 to 65±4 ka and all are identified as well or probably well-bleached (Table 2). The sediment sequence began to be deposited in MIS 4 (65±4 ka) but soil development did not take place until after 54±4 ka, when a well-developed palaeosol (Btk 45-70 cm) began to form. The upper unit was deposited at 18±1.1 ka during MIS 2, and so the underlying soil probably developed during MIS 3.

The Isfahan section consists of a multiple pedocomplex. The OSL age estimates range from 40±8 for a sample from the upper horizon at 50 cm below the surface to 107±11 ka for the sedimentary unit at 140 cm (ignoring the unit below this for the reasons discussed above). All of the samples are judged to have been well-bleached or probably-well bleached before deposition (Table 2). The sediment sequence began to be deposited at 107±11 ka or earlier and soil formation occurred later, but before 73±6 ka, when more sediment was deposited covering the palaeosol. Further pedogenesis occurred after this time, but before 40±8 ka, when more sediment was deposited. One final period of soil development is recorded at the top of this section, occurring after 40±8 ka. This palaeosol presumably developed at the same time as that found in the middle unit at Mahan (deposition at 54±4 ka), and possibly the bottom unit at Bam (deposition at 61±5 ka). Thus, it appears we have 4 periods of soil

development represented at Isfahan, the first (bottom unit) of unknown age but before MIS 5d, one during mid/late MIS 5, one between MIS 5 and mid MIS 3, and the top palaeosol during late MIS 3.

The Lar section is similar to that at Isfahan. The earliest sediment deposition occurs at 102±10 ka. This unit is covered by one deposited at 73±12 ka, which is in turn covered by one from 43±5 ka. Unfortunately, feldspar was unavailable for these samples, and so we are unable to comment on the degree of bleaching prior to deposition. Each sedimentary unit contains a well-developed palaeosol, and thus, as with Isfahan, there are soil formation periods during mid/late MIS 5, one between MIS 5 and mid MIS 3, and one after mid MIS 3.

In summary, we have firm evidence for soil formation before MIS 5d, during mid/late MIS 5, between MIS 5 and mid MIS 3, but probably in early MIS 3 (because of the constraining 54±4 ka age at Mahan), during late MIS 3, and in the early to mid MIS 1.

8. Conclusion

For the first time, a chronology has been developed for the sediments hosting several soil profiles in the central Iranian plateau. Our OSL ages indicate the time at which the sediment was deposited; soil formation took place later. The 17 OSL ages constrain at least four broad phases of sediment deposition and soil formation on the central Iranian plateau: (i) prior to, and (ii) during, mid/late MIS 5 (at Isfahan and Lar), (iii) MIS 3 (at Bam, Mahan and probably Isfahan), and (iv) MIS 1 (at Rayen and Jiroft). It appears that, over the last full glacial-interglacial cycle, there is no convincing evidence for palaeosol formation during MIS 4 and MIS 2.

Acknowledgements

ZR would like to thank Aarhus University and the Ministry of Science, Research and Technology of Islamic Republic of Iran for financial support during her visit to Denmark.

References

Bøtter-Jensen, L., Thomsen, K., Jain, M. 2010. Review of optically stimulated luminescence (OSL) instrumental developments for retrospective dosimetry. Radiation Measurements 45, 253-257.

Büdel, C., Padashi, S.M., Hoelzmann, P., Fuchs, M., Baumhauer, R., 2017. The correlation of North-Iranian Late Pleistocene and Holocene playa sediments to basin geomorphology. Zeitschrift für Geomorphologie 61, 77-99.

Buylaert, J.P., Jain, M., Murray, A.S., Thomsen, K.J., Thiel, C., Sohbati, R. 2012. A robust feldspar luminescence dating method for Middle and Late Pleistocene sediments. Boreas 41, 435-451.

Chapot, M.S., Roberts, H.M., Duller, G.A.T. and Lai, Z.P., 2012. A comparison of natural- and laboratory-generated dose response curves for quartz optically stimulated luminescence signals from Chinese Loess. *Radiation Measurements*, *47*(11-12), 1045-1052.

Cunningham A.C., Wallinga, J. 2010. Selection of integration time intervals for quartz OSL decay curves. Quaternary Geochronology 5, 657-666.

Darehshouri, B. and Kasraian, N. 1998. Nature of Iran, Rozane-kar Press, p10.

Duller, G.A.T. 2003. Distinguishing quartz and feldspar in single grain luminescence measurements. Radiation Measurements 37, 161-165.

Farpoor, M.H., Neyestani, M., Eghbal, M.K., Esfandiarpour Borujeni, I. 2012. Soil geomorphology relationships in Sirjan playa, south central Iran. Geomorphology 138, 223-230.

Frechen, M., Kehl, M., Rolf, C., Sarvati, R., Skowronek, A. 2009. Loess chronology of the Caspian Lowland in northern Iran. Quaternary International 128, 220-233.

396 Ghafarpour, A., Khormali, F., Balsam, W., Karimi, A., Ayoubi, S. 2016. Climatic
397 interpretation of loess-paleosol sequences at Mobarakabad and Aghband, Northern Iran.
398 Quaternary Research 86, 95-109.
399 Godfrey-Smith, D.L., Huntley, D.J., Chen, W.H. 1988. Optically dating studies of quartz and
400 feldspar sediment extracts. Quaternary Science Reviews 7, 373-380.
401 Gornitz, V. 2008. Encyclopedia of Paleoclimatology and Ancient Environments, New York,
402 Springer, Encyclopedia of Earth Sciences Series, 1049 p.
403 Guerin, G., Mercier. N., Adamiec, G. 2011. Dose-rate conversion factors: update. Ancient TL
404 29, 5-8.
405 Hall, S. A. and Goble, R. J. 2015. OSL age and stratigraphy of the Strauss sand sheet in New
406 Mexico, USA. Geomorphology 241, 42-54.
407 Hansen, V., Murray A.S., Buylaert J.P., Yeo, E., Thomsen, K. 2015. A new irradiated quartz
408 for beta source calibration. Radiation Measurements 81: 123-127.
409 Huntley, D. and Baril, M. 1997. The K content of the K-feldspars being measured in optical
410 dating or in thermoluminescence dating. Ancient TL 15, 11–13.
411 Huntley, D., Hancock, R. 2001. The Rb contents of the K-feldspar grains being measured in
412 optical dating. Ancient TL 19, 43–46.
413 Jain, M., Murray, A. S., Bøtter-Jensen, L. 2003. Characterisation of bluelight stimulated
414 luminescence components in different quartz samples: implications for dose
415 measurement. Radiation Measurements 37, 441-449.
416 Jain, M., Murray, A.S., Bøtter-Jensen, L. 2004. Optically stimulated luminescence dating:
417 how significant is incomplete light exposure in fluvial environments? Quaternaire 15,
418 143-157.
419 Karimi, A., Frechen, M., Khademi, H., Kehl, M., Jalalian, A. 2011. Chronostratigraphy of
420 loess deposits in northeast Iran. Quaternary International 234, 124-132.

421 Karimi, A., Khademi, H., Kehl, M., Jalalian, A. 2009. Distribution, lithology and provenance
422 of peridesert loess deposits in northeastern Iran. Geoderma 148, 241-250.
423 Kehl, M. 2010. Quaternary loesses, loess-like sediments, soils and climate change in Iran.
424 Relief Boden Paläoklima, Band 24, 209 p.
425 Kehl, M., Frechen, M., Skowronek, A. 2009. Nature and age of Late Quaternary basin fill
426 deposits in the Basin of Persepolis/Southern Iran. Quaternary International 196, 57-70.
427 Kehl, M., Frechen, M., Skowronek, A., 2005. Paleosols derived from loess and loess-like
428 sediments in the Basin of Persepolis, Southern Iran. Quaternary International 140/141,
429 135-149.
430 Kemp, R. A., Zárate, M., Toms, P., King, M., Sanabria, J., Arguello, G. 2006. Late
431 Quaternary paleosols, stratigraphy and landscape evolution in the Northern Pampa,
432 Argentina. Quaternary Research 66, 119-132.
433 Khademi, H., Mermut, A.R. 1999. Submicroscopy and stable isotope geochemistry of
434 carbonate and associated palygorskite in Iranian Aridisols. European Journal of Soil
435 Science 50, 207-216.
436 Khormali, F., Abtahi, A., Mahmoodi, S., Stoops, G. 2003. Argillic horizon development in
437 calcareous soils of arid and semiarid regions of southern Iran. Catena 53, 273-301.
438 Khormali, F., Kehl, M. 2011. Micromorphology and development of loess-derived surface
439 and buried soils along a precipitation gradient in Northern Iran. Quaternary
440 International 234, 109-123.
441 Kraus, M.J. 1999. Paleosols in clastic sedimentary rocks: their geologic applications. Earth
442 Science Reviews 47, 41-70.
443 Lauer, T., Vlaminck, s., Frechen, M., Rolf, C., Kehl, M., Sharifi, J., Lehndorff, E., Khormali,
444 F. 2016. The Agh Band loess-palaeosol sequence e A terrestrial archive for climatic

445 shifts during the last and penultimate glacialeinterglacial cycles in a semiarid region in
446 northern Iran. Quaternary International 429(B), 13-30.
447 Leopold, M., Völkel, J., Dethier, D., Huber, J., Steffens, M. 2011. Characteristics of a
448 paleosol and its implication for the Critical Zone development, Rocky Mountain Front
449 Range of Colorado, USA . Applied Geochemistry 26, S72-S75.
450 Li, B., Li, S. 2006. Comparison of estimates using the fast component and the medium
451 component of quartz OSL. Radiation Measurements 41, 125-136.
452 Mahaney, W.C., Barendregt, R. W., Hamilton, T. S., Hancock, R. G. V., Tessler, D., Costa,
453 P. J.M. 2013. Stratigraphy of the Gorges moraine system, Mount Kenya: palaeosol and
454 palaeoclimate record. Journal of the Geological Society, London 170, 497-511.
455 Mejdahl, V. 1987. Internal radioactivity in quartz and feldspar grains. Ancient TL 5, 10-17.
456 Murray, A.S. and Wintle, A.G. 2000. Luminescence dating of quartz using an improved
457 single-aliquot regenerative-dose protocol. Radiation Measurements 32, 57-73.
458 Murray, A.S. and Wintle, A.G. 2003. The single aliquot regenerative dose protocol: potential
459 for improvements in reliability. Radiation Measurements 37, 377-381.
460 Murray, A.S., Clemmensen, L.B. 2001. Luminescence dating of Holocene aeolian sand
461 movement, Thy, Denmark. Quaternary Science Reviews 20, 751-754.
462 Murray, A.S., Marten, R., Johnston, A., Martin, P. 1987. Analysis for naturally occurring
463 radionuclides at environmental concentrations by gamma spectrometry. Journal of
464 Radioanalytical and Nuclear Chemistry 115, 263-288.
465 Murray, A.S., Olley, J.M. 2002. Precision and accuracy in the optically stimulated
466 luminescence dating of sedimentary quartz. Geochronometria 21, 1-16.
467 Murray, A.S., Thomsen, K.J., Masuda, N., Buylaert, J.P., Jain, M. 2012. Identifying well-
468 bleached quartz using the different bleaching rates of quartz and feldspar luminescence
469 signals. Radiation Measurements 47, 688-695.

Nejadzamani, L., 2014. Soil–geomorphology relationships in Rayen, Kerman. Master thesis of Bahonar University of Kerman (in Persian).

Porat, N., Amit, R., Enzel, Y., Zilberman, E., Avni, Y., Ginat, H., Gluck, D. 2010. Abandonment ages of alluvial landforms in the hyperarid Negev determined by luminescence dating. Journal of Arid Environments 74, 861-869.

Prescott, J. Hutton, J. 1994. Cosmic ray contributions to dose rates for luminescence and ESR dating: large depths and long-term time variations. Radiation Measurements 23, 497-500.

Retallack, G.J., 2001. Soils of the Past. An Introduction to Paleopedology. Blackwell.

Sanjari, S,. Farpoor, M.H., Eghbal, M.K., Esfandiarpour Borujeni, I. 2011. Genesis, micromorphology and clay mineralogy of soils located on different geomorphic surfaces in Jiroft area. Journal of Water and soil 20, 411-428 (in Persian).

Sohbati, R., Borella, J., Murray, A.S., Quigley, M., Buylaert, J.P. 2016. Optical dating of loessic hillslope sediments constrains timing of prehistoric rockfalls, Christchurch, New Zealand. Journal of Quaternary Science 31, 678-690.

Soil Survey Staff, 2014. Keys to Soil Taxonomy, 14th edition. U.S. Department of Agriculture, Natural Resources Conservation Service.

Vandenberghe D, De Corte F, Buylaert J.P., Kucera, J., Van den hautea, P. 2008. On the internal radioactivity in quartz. Radiation Measurements 43, 771-775.

Wang, X., Wei, H., Taheri, M., Khormali, F., Danukalova, G., Chen, F. 2016. Early Pleistocene climate in western arid central Asia inferred from loess-palaeosol sequences. Scientific Reports 6, Article number: 20560.

Figure captions

Figure 1) (a) Map of the Middle East and Iran, showing the location of six sampling sites in the (semi-)arid zones of Iranian plateau. (b) Stratigraphy of palaeosol units and location of the OSL samples. The dashed lines indicate possible chronological correlations, not coeval soil development. There are marked discontinuities in all profiles. These may be erosional.

Figure 2) Summary of luminescence characteristics of quartz OSL signal. (a) Typical dose-response and stimulation (inset) curves, (b) and (c) natural and dose recovery preheat plateau tests for a sample from Mahan (171118). Each data point represents the average of three aliquots. The error bars show one standard error. Inset to (c) shows the summary of dose recovery test for all the samples in this study.

Figure 3) (a) Sample-averaged K-feldspar equivalent doses. Error bars represent one standard error, (b) quartz OSL and K-feldspar IR_{50} ages, (c) quartz OSL and K-feldspar $pIRIR_{290}$ ages, (d) quartz OSL to K-feldspar IR_{50} age ratio plotted against quartz dose recovery ratio.

520

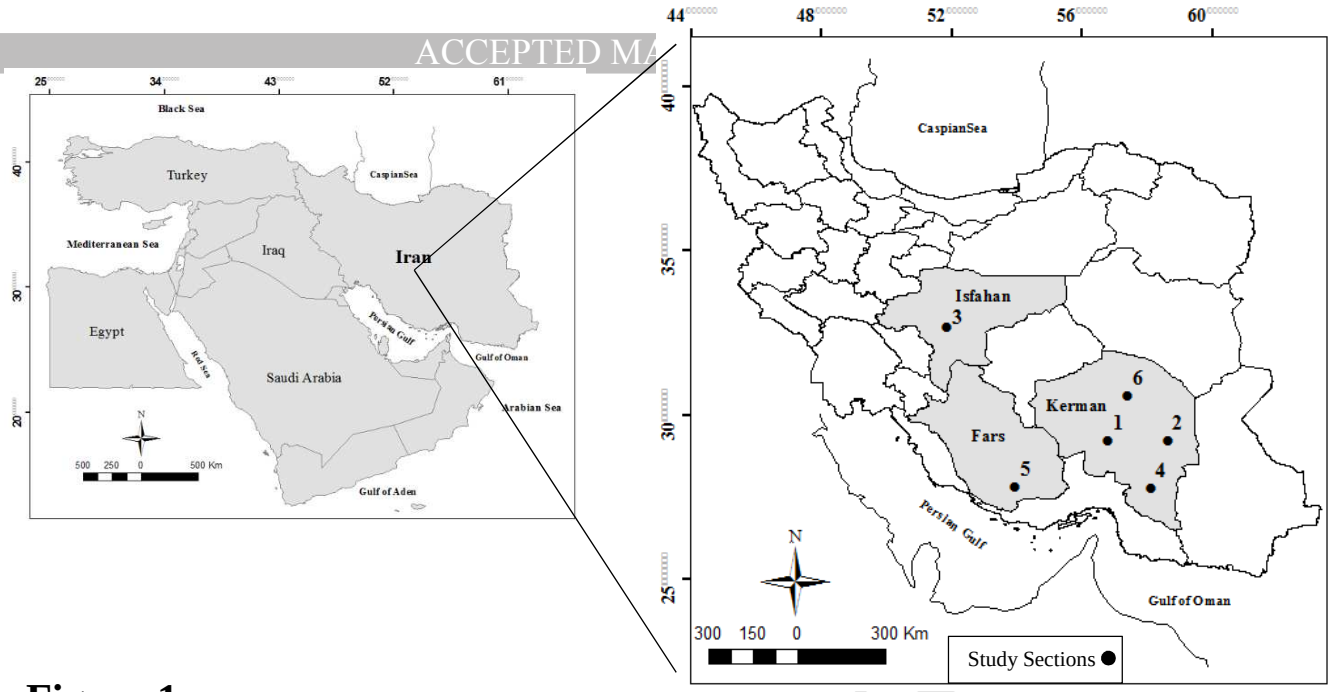

Figure 1a

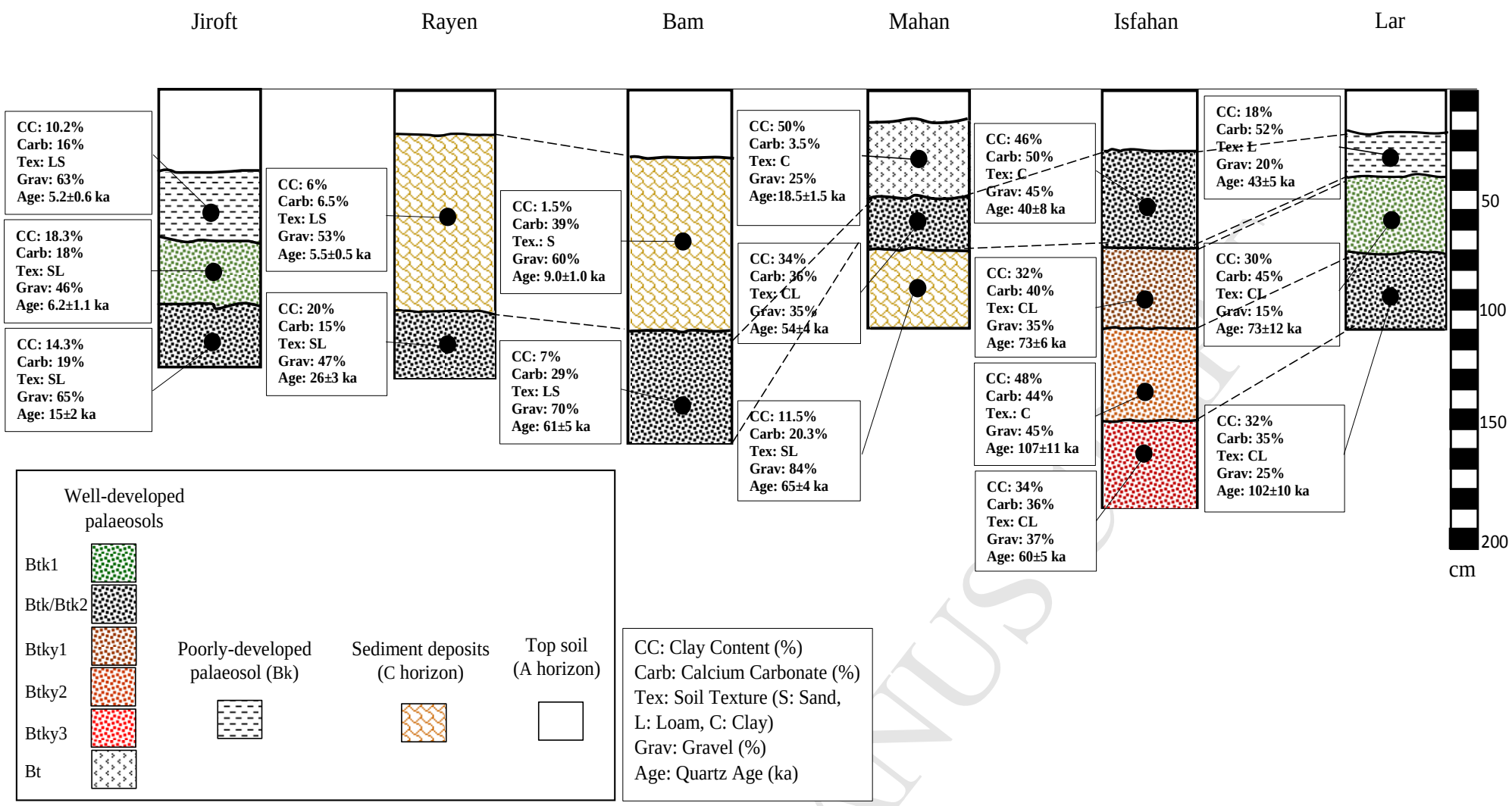

Figure 1b

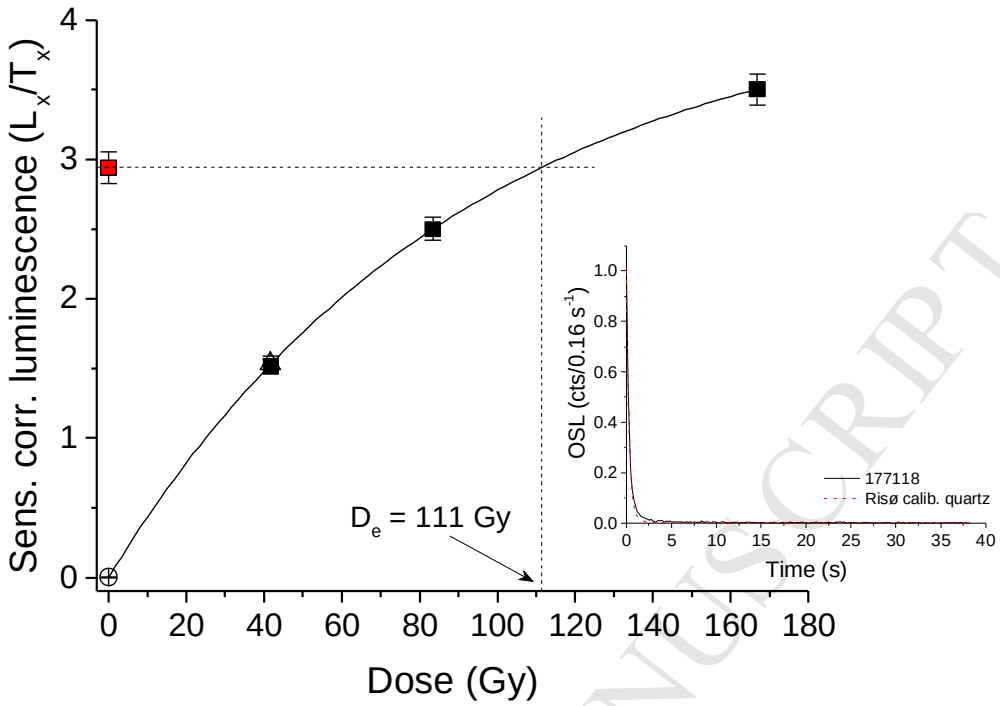

Figure 2a

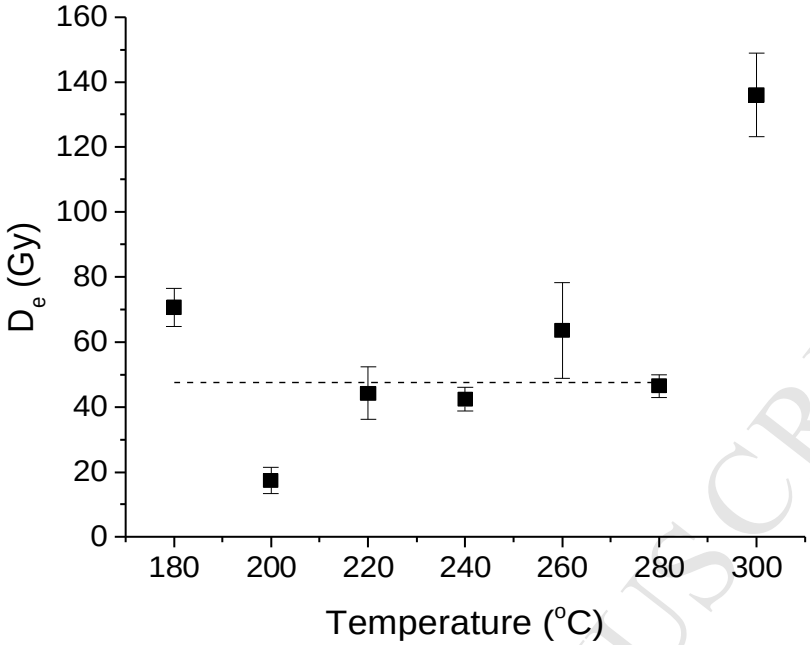

Figure 2b

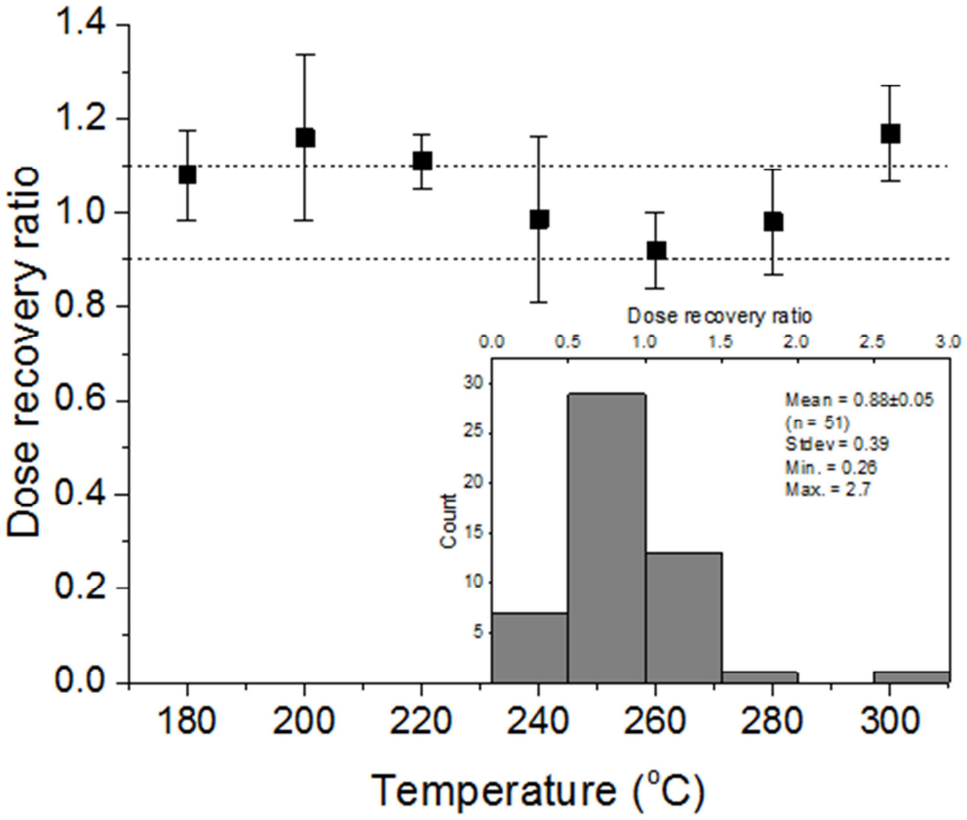

Figure 2c)

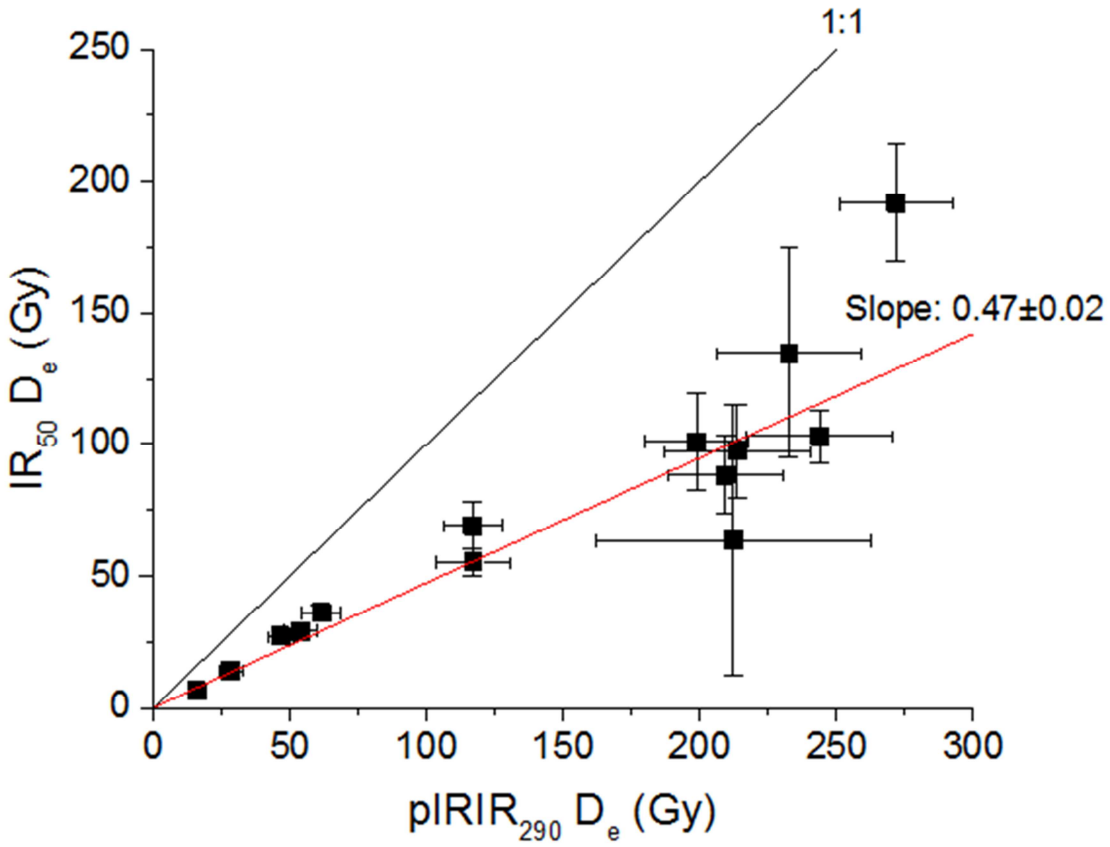

Figure 3a)

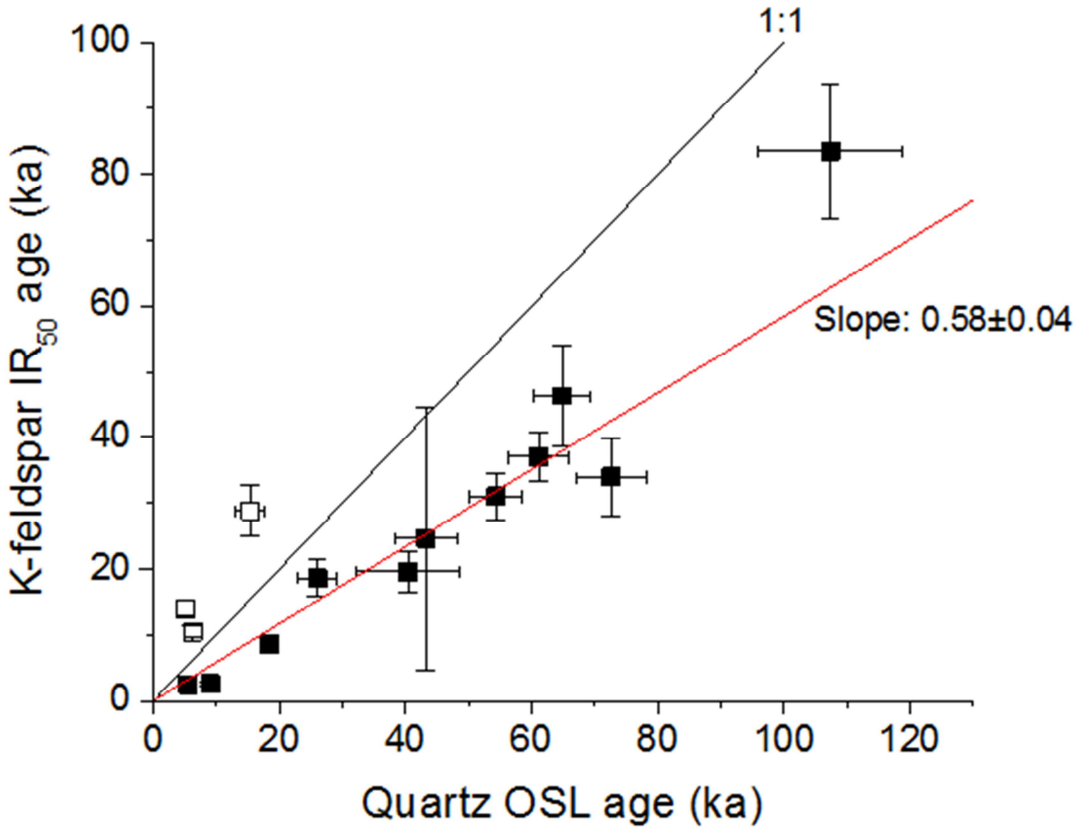

Figure 3b)

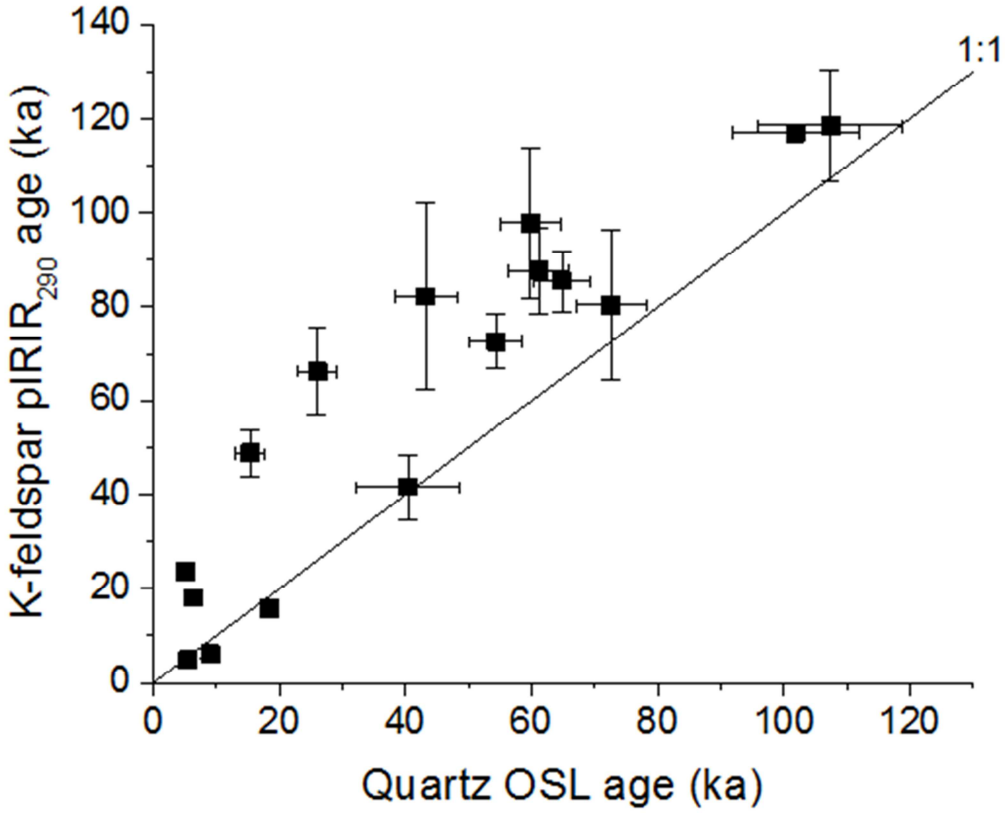

Figure 3c)

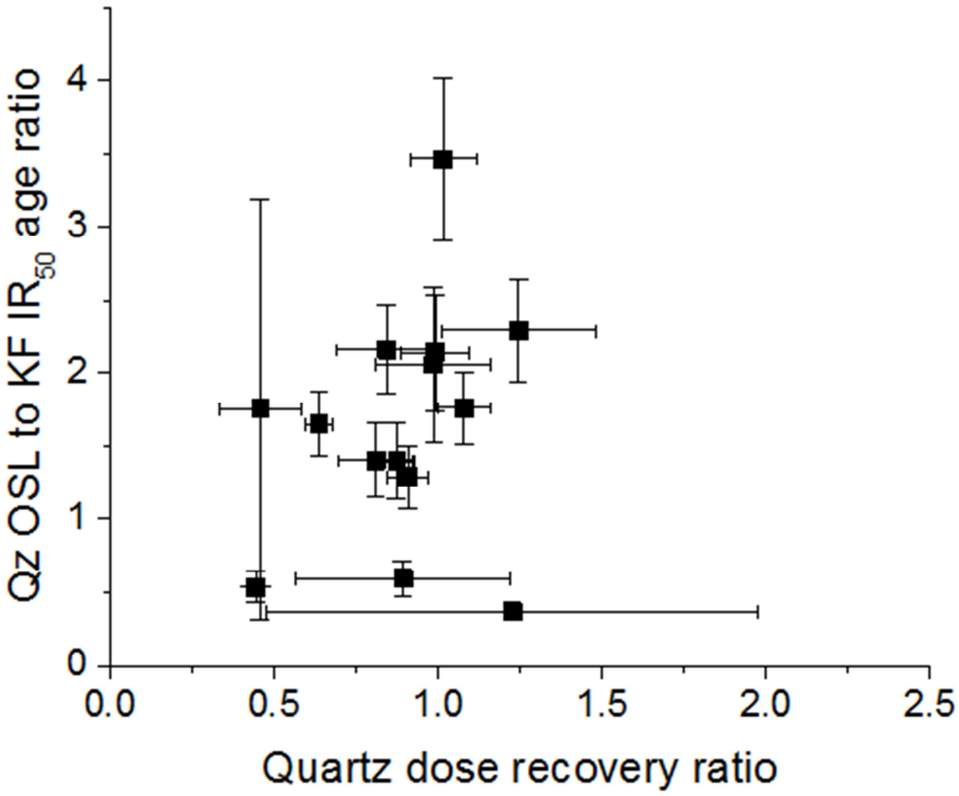

Figure 3d)

Table 1

Sampling locations and pedological description of sections

Section	Longitude (E)	Latitude (N)	Altitud (m)	Mean annual precipitation (mm)	Mean annual temperature (mm)	Landform	local geology	Sediment origin geology
Rayen	57° 39′ 21′′	29° 27′ 25′′	2328	200	14	Pediment	Quaternary older gravel fan	Middle Eocene Igneous Rocks and Eocene marl
Bam	57° 39′ 39′′	29° 39′ 55′′	2096	145	15.5	Pediment	Upper Neogene to Quaternary conglomerate, sandstone	Cretaceous marl, sandstone and Paleocene to Eocene gypsiferous marl
Isfahan	51° 51′ 21′′	32° 40′ 64′′	1598	150	14.7	Alluvial fan	Oligo-Miocene limestone	Cretaceous limestone
Jiroft	57° 42′ 50′′	28° 37′ 53′′	660	185	24.5	fluvial plain	Recent alluvium, river terraces	Miocene to Pliocene marl, limestone and conglomerate
Lar	53° 57′ 19′′	27° 47′ 23′′	1071	170	23.3	Plateau	Miocene-Pliocene gypseous marl, calacareous sandstone	Eocene limestone and marl
Mahan	57° 17′ 23′′	30° 08′ 38′′	1912	160	14.5	Alluvial fan	Quaternary conglomerate and older fanglomerate deposits	Upprt Cretaceous limestone and gypsiferous marl

Table 2

Summary of sample code, burial depth, radionuclide concentrations, measured water content, quartz OSL and K-feldspar IR_{50} and $pIRIR_{290}$ equivalent doses. Feldspar dose rates assume a K concentration of 12.5±0.5% for K-feldspar (Huntley and Baril, 1997). An absolute error of 4% is assumed on the water content values.

section	Sample code	Depth (cm)	Water content (%)	^{226}Ra ($Bqkg^{-1}$)±se	^{232}Th ($Bqkg^{-1}$)±se	^{40}K ($Bqkg^{-1}$)±se	Total dose rate ($Gyka^{-1}$)±se	Quartz OSL De (Gy)±se	n	Quartz OSL age (ka)±se	K-feldspar IR_{50} D_e (Gy)±se	K-feldspar IR_{50} age (ka)±se	K-feldspar $pIRIR_{290}$ D_e (Gy)±se	n	K-feldspar $pIRIR_{290}$ age (ka)±se	Age ratio IR_{50}/OSL	Age ratio $pIRIR_{290}$/OSL	Well bleached	Probably well bleached
Rayen	177107	60	1	37.6±0.64	54.7±0.83	966±19.0	4.79±0.22	27±2	18	5.5±0.5	13.9±1.5	2.4±0.3	28±2.85	9	4.9±0.5	0.44±0.06	0.9±0.12	√	√
	177108	115	2	49.6±1.11	70.0±1.01	815±20.0	4.71±0.22	125±10	17	26±3	105.4±14	19±3	375±49	20	66± 9	0.71±0.13	2.5±0.45		√
Bam	177111	70	1	19.5±0.48	14.7±0.37	256±8.0	1.64±0.07	14.7±1.5	17	9.0±1.0	6.6±0.86	2.6± 0.3	15.8±2.4	17	6.1± 1.0	0.29±0.04	0.68±0.13	√	√
	177112	150	4	22.3±0.45	19.5±0.40	310±8.0	1.84±0.08	112±7	16	61±5	103±9.9	37± 4	243.9±22	11	88± 9	0.61±0.08	1.4±0.18		√
Isfahan	177118	50	4	26.6±1.00	16.1±0.7	310±14.9	1.87±0.35	76±6	22	40±8	55±5	20± 3	117±11.4	12	42± 7	0.5±0.12	1.03±0.27	√	√
	177119	95	1	26.2±0.83	13.3±0.6	253±12.0	1.67±0.08	121±7	16	73±6	88.3±14.7	34± 6	209±40.7	6	80± 16	0.47±0.08	1.1 ±0.23	√	√
	177120	140	2	24.1±0.39	10.1±0.2	186±5.0	1.36±0.06	148±14	17	107±11	191.7±22	84± 10	271.9±24.5	2	119± 12	0.8±0.12	1.1±0.16	√	√
	177121	160	2	24.4±0.30	11.8±0.2	201±4.0	1.44±0.06	86±6	15	60±5	134.86±39.7	57±17	232.6± 37	17	98± 16	0.95±0.3	1.1±0.16	√	√
Jiroft	177125	60	4	17.3±0.81	14.0±0.6	313±14	1.65±0.08	8.5±0.9	16	5.2±0.6	36.1±2.6	14±1.2	61.4±3.9	17	24± 1.8	2.7±0.38	4.6±	?	
	177126	85	3	15.2±0.25	13.6±0.2	328±5	1.65±0.07	10.3±1.8	16	6.2±1.1	27±2.2	10.5±0.9	46.6±4	14	18± 1.7	1.67±0.33	2.9±	?	
	177127	115	1	11.9±0.26	11.3±0.3	290±6	1.46±0.06	22±3	24	15±2	69.8±8.7	29± 4	116.8± 10.6	18	49± 5	1.9±0.37	3.3±	?	
Lar	177129	30	8	53.9±0.64	9.09±0.3	138±6	1.64±0.08	71±7	20	43±5	63.59±51.5	24.6±20	212±50.2	4	82±20	0.57±0.47	1.9±0.51		√
	177130	60	4	32.3±0.51	5.5±0.4	89±4	1.07±0.05	79±13	9	73±12	-	-	-	0	-	-	-		
	177128	95	5	35.02±0.61	6.18±0.35	99±6	1.2±0.05	122±10	14	102±10	-	-	249.14	1	117	-	1.15±0.11		
Mahan	177131	30	1	26.4±0.83	24.6±0.7	426±14	2.47±0.11	46±3	20	18.5±1.5	29±3.2	8.5± 1.0	53.9±3.4	15	15.8± 1.2	0.46±0.06	0.86±0.09	√	√
	177132	60	2	21.9±0.51	18.3±0.5	281±9	1.8±0.08	98±6	18	54±4	84.6±9.5	31± 4	198.7±13	13	73± 6	0.57±0.08	1.34±0.15		√
	177133	90	1	18.2±0.52	15.3±0.5	241±8	1.56±0.07	101±5	21	65±4	115.6±18.7	46± 8	213± 13.2	11	86± 6	0.71±0.13	1.33±0.13		√

Table 3

Quartz OSL, feldspar IR_{50} and feldspar $pIRIR_{290}$ apparent residual doses in modern analogue samples

Sample	Type	Quartz (Gy)	IR_{50} (Gy)	$pIRIR_{290}$ (Gy)
Rayen	Alluvial	1.64± 0.3	0.7± 0.2	4.7± 1.9
Bam	Alluvial	0.11± 0.02	0.4± 0.2	1.9± 0.5
Jiroft	Fluvial	1.2± 1.01	1.4± 0.2	2.4± 0.5
Lar	Alluvial	0.11± 0.02	0.51± 0.15	2.8± 0.47
Mahan	Alluvial	0.1± 0.01	2.3± 1.9	3.5± 1.02

Supplementary materials

Fig S1

The photo shows the typical topography of our sampling sites

Table S1

Outline of the SAR OSL and post-IR IRSL protocol (Murray and Wintle, 2003; Buylaert et al. 2012)

step	Quartz		K-feldspar	
	Treatment	Observed	Treatment	Observed
1	Dose		Dose	
2	Preheat (240℃ for 10 s)		Preheat (320℃ for 60 s)	
3	Blue stimulation (125℃ for 40 s)	L_x	Infrared stimulation (50℃ for 100 s)	L_x, IR_{50}
4	-		Infrared stimulation (290℃ for 100 s)	L_x, $pIRIR_{290}$
5	Test dose		Test dose	
6	Cut heat (290℃ for 0 s)		Preheat (320℃ for 60 s)	
7	Blue stimulation (125℃ for 40 s)	T_x	Infrared stimulation (50℃ for 100 s)	T_x, IR_{50}
8	-		Infrared stimulation (290℃ for 100 s)	T_x, $pIRIR_{290}$
9	Blue stimulation (280℃ for 40 s)		Infrared stimulation (325℃ for 100 s)	
10	Return to 1		Return to 1	